NJC

ROYAL SOCIETY OF CHEMISTRY

PAPER

View Article Online
View Journal | View Issue

Cite this: *New J. Chem.*, 2022, **46**, 5515

A binuclear Fe(III)/quinizarin complex as a structural model for anthracycline drugs binding to iron†

Juliana S. do Nascimento,[a] Aurideia P. de Sousa,[a] Ana C. S. Gondim,[a] Eduardo H. S. Sousa,[a] Edson H. Teixeira,[b] Luiz Gonzaga do Nascimento Neto,[c] Beatriz Pinheiro Bezerra,[d] Alejandro Pedro Ayala,[d] Alzir A. Batista,[e] Igor F. Vasconcelos,[f] Francisco G. S. Oliveira[f] and Alda K. M. Holanda *[a]

Received 25th August 2021,
Accepted 7th February 2022

DOI: 10.1039/d1nj04087a

rsc.li/njc

The *cis*-[Fe(cyclam)Cl_2]Cl (cyclam = 1,4,8,11-tetraazacyclotetradecane) complex reacts with quinizarin (1,4-dihydroxy-9,10-anthraquinone, Qz), a biologically relevant molecule, yielding the binuclear complex [(Fe(cyclam))$_2$(Qz)]Cl$(PF_6)_3$. This new compound was characterized by means of elemental analysis, X-ray diffraction, cyclic voltammetry and spectroscopic techniques. Crystallographic and FTIR data indicated that the bridging ligand, quinizarin, is coordinated to the Fe^{III} cation *via* the oxygen atoms of the carbonyl groups in the form of quinones. The effect of ancillary (cyclam) and bridging (Qz) ligands on the properties of the complex is reflected by the stabilization of the Fe^{III}–Fe^{III} configuration supported by Mössbauer spectroscopy. The efficiency of ROS generation and DNA cleavage activity for this binuclear complex, as well as for the free quinizarin ligand, were investigated. This metal complex exhibited very low photochemical activity; however, it revealed a great ability to cleave the DNA molecule in the presence of glutathione, which was associated with the production of ROS species. Thereafter, the cytotoxic activity of these compounds was evaluated using the MTS assay against human tumor cells, namely lung adenocarcinoma (A549) and prostate carcinoma (LNCaP clone FGC), and against normal fibroblasts (L929). Our findings indicated low cytotoxic effects in general, where only a slight reduction in A549 and L929 cell viability was observed after light irradiation. Despite the lack of any significant biological activity, this binuclear compound validates *in vitro* the essential role of metal binding to an anthracycline-like moiety in the generation of ROS. The latter may be responsible for some of the cardiotoxicity reported for anthracycline-based drugs.

1 Introduction

Anthracyclines are a class of antineoplastic drugs derived from *Streptomyces* sp. First, anthracyclines were isolated from *Streptomyces peucetius* and named doxorubicin and daunorubicin. These drugs have been in clinical use for nearly 5 decades in the treatment of various human cancers, including breast, ovarian, lung, and a wide range of neuroblastomas and leukemia.[1–5] The mechanism of action of anthracyclines is related to the induction of oxidative stress, intercalation in DNA, and, more importantly, poisoning of the topoisomerase II enzyme (Top2).[6–8] However, anthracyclines are also tempered by toxic side effects, including hair loss, bone marrow suppression, vomiting, rash and allergic reactions.[6] Besides that, the most harmful side effect of doxorubicin is dilated cardiomyopathy, leading to congestive heart failure.[9] The mechanisms underlying anthracycline-dependent cardiotoxicity are multiple and remain poorly understood, but many observations indicate that interactions with cellular iron are important. It is already known that the hydroxyquinone moiety found in anthracycline drugs binds easily to metals. Indeed, these types of drugs are recognized as good iron chelators, capable of acquiring iron from ferritin or transferrin in acidic intracellular compartments.[10] The negative

[a] *Laboratório de Bioinorgânica, Departamento de Química Orgânica e Inorgânica, Universidade Federal do Ceará, PO Box 12200, Campus do Pici s/n, 60440-900, Fortaleza, CE, Brazil. E-mail: aldakarine@dqoi.ufc.br*
[b] *Laboratório Integrado de Biomoléculas, Departamento de Patologia e Medicina Legal, Universidade Federal do Ceará, CEP 60430-270, Fortaleza, CE, Brazil*
[c] *Departamento do Núcleo Comum, Instituto Federal de Educação, Ciência e Tecnologia do Ceará, Campus Limoeiro do Norte s/n, 62930-000, Limoeiro do Norte, CE, Brazil*
[d] *Department of Physics, Federal University of Ceara, Fortaleza, CE, Brazil*
[e] *Departamento de Química, Universidade Federal de São Carlos, PO Box 676, 13565-905 São Carlos, SP, Brazil*
[f] *Departamento de Engenharia Metalúrgica e de Materiais, Centro de Tecnologia, Universidade Federal do Ceará, Campus do Pici, Bloco 729, 60440-900, Fortaleza, CE, Brazil*

† Electronic supplementary information (ESI) available. CCDC 2005420. For ESI and crystallographic data in CIF or other electronic format see DOI: 10.1039/d1nj04087a

charge of doxorubicin facilitates good affinity towards the iron cation and forms a doxorubicin-Fe complex, which might further react with free oxygen and catalytically generate ROS species.[11,12] These species could account for most of the known cytotoxic effects of the drug, such as damage to DNA and cell membranes, as well as cardiotoxicity. To explore the nature of the metal complexes formed between anthracycline drugs and biological molecules containing iron, some studies have reported the use of quinizarin (Qz) to model the dihydroxyquinone moiety found in these drugs.[13] However, in the literature there are only a few known examples of this type of iron complex. In this context, the metal complex $[Fe(salen)]_2Qz$ was probably the first structurally characterized compound with direct structural relevance to iron binding by anthracycline drugs.[14] Regarding the simpler structural model of the anthracyclines, quinizarin, dinuclear Ru(III), Os(II) and Co(III) complexes containing quinizarin as a bridging ligand were also synthesized and characterized.[15–17] In all cases, the redox study of the metal complexes revealed the non-innocent behavior of the anthraquinone ligand and several oxidation and reduction steps of the compound were described. Based on that, this work aimed to synthesize and characterize a new binuclear Fe(III) complex bearing Qz as a model for anthracycline drugs, in order to explore its stability, kinetics and redox behavior. In addition, we chose 1,4,8,11-tetraazacyclotetradecane (cyclam) as an ancillary macrocyclic ligand as it can form more stable metal complexes compared to chelating open chain ligands.[18] We also investigated the efficiency of this new compound to respond to light and glutathione, and its ability to cause damage to DNA. Moreover, the effect of the binuclear complex on the cellular viability of two cancer cell lines, LNCaP (prostate cancer) and A549 (lung cancer), and a normal cell line L929 (mouse fibroblast) was also investigated using the MTS [3-(4,5-dimetiltiazol-2-il)-5-(3-carboximetoxifenil)-2-(4-sulfofenil)-2*H*-tetrazolium] assay.

2 Experimental

2.1. Materials

Ultrahigh pure water from a Millipore system (model: Millipore Direct Q® 3UV) was used throughout the experiments. All chemicals, purchased from Sigma/Aldrich/Merck, were reagent grade or comparable in purity, and were used as received. The *cis*-$[Fe(cyclam)Cl_2]Cl$ complex was prepared according to the procedure in the literature.[19] Salmon sperm DNA was purchased from Sigma-Aldrich and pBR322 plasmid from New England Biolabs (USA). For the cell culture, phosphate buffered saline (PBS; pH 7.4), heat-inactivated fetal bovine serum (FBS), L-glutamine (200 mM), trypsin/EDTA solution (TE) and penicillin–streptomycin were purchased from Gibco® by life Technologies. Roswell Park Memorial Institute 1640 medium (RPMI 1640) and Dulbecco's modified Eagle medium (DMEM) were purchased from Merck®. Moreover, CellTiter 96® Aqueous MTS Reagent Powder was purchased from Promega Inc.

2.2. Synthesis of the $[(Fe(cyclam))_2(Qz)]Cl(PF_6)_3$ complex

To prepare the binuclear metal complex, a solution of 0.112 mmol of *cis*-$[Fe(cyclam)Cl_2]Cl$ in distilled water (50 mL) was mixed with 0.125 mmol of quinizarin in acetone (20 mL) and stirred for approximately 3 hours under reflux (*ca.* 50 °C). After this time, the flask was opened allowing approximately 10 mL of the acetone to evaporate, leading to the precipitation of excess of quinizarin. This orange crystalline ligand was then separated out through filtration. The binuclear complex that remained dissolved in the mother liquor was then precipitated by adding saturated NH_4PF_6 in water (*ca.* 1 mL). The violet crystalline complex was then separated out through filtration and dried under vacuum. Yield = 68 mg or 69% (based on the iron cyclam used). Elemental analysis: anal. calc. for $[C_{34}H_{54}ClF_{18}Fe_2N_8O_4P_3]$: exp. (calc.) C, 33.50 (33.44); H, 4.41 (4.46); N, 9.26 (9.18)%.

2.3. Instrumentation

FTIR spectra were obtained as KBr pellets using an ABB Bomem FTLA 2000-102 spectrophotometer. Electrochemical experiments were performed with a potentiostat Epsilon model E2-818 (BAS Inc.) at 25 °C using a conventional three-electrode glass cell with platinum, Ag|AgCl and glassy carbon as the auxiliary, reference and working electrodes, respectively. For electrochemical measurements in organic medium the supporting electrolyte used was tetrabutylammonium perchlorate (PTBA) at 0.1 mol L^{-1} in HPLC grade acetonitrile (MeCN), and ferrocene was used under these conditions as an internal reference, whose redox potential was at 0.43 V (Fc^+/Fc). The electronic spectra used for characterization of the metal complex and Qz ligand were acquired with a HP-8453 diode-array spectrophotometer in different solvents: methanol, acetonitrile, water and dimethyl sulfoxide. UV/Vis/NIR spectroelectrochemical studies were performed in CH_3CN/0.1 M PTBA, at 298 K. For spectroelectrochemical experiments, a potentiostat model 910 PSTAT (Metrohm Autolab, Utrecht, the Netherlands) using an optically transparent thin-layer cell (1 mm; BAS Inc., Eatonville, WA, USA) with platinum mesh, platinum wire, and Ag|AgCl|Cl^- as the working, counter and reference electrodes, respectively, was used. A Cary 5000 UV-vis-NIR spectrophotometer was used to acquire the spectra. The room temperature Mössbauer spectrum was measured in transmission mode using a ^{57}Co(Rh) radioactive source mounted on a velocity driver operating in sinusoidal mode. The data were evaluated by least square fitting to a series of discrete Lorentzian-shaped subspectra by means of the software package Normos. Isomer shifts (δ) are reported with respect to α-Fe.

2.4. X-Ray diffraction

Single crystals were obtained by slow evaporation of a methanol/ether solution and X-ray diffraction data collection (φ scans and ω scans with κ and θ offsets) was recorded on a Bruker D8 Venture κ-geometry diffractometer equipped with a Photon II CPAD detector and a IμS 3.0 Incoatec [Cu Kα (λ = 1.54178 Å)] microfocus source. Data collections were performed at 150 K using an Oxford Cryostream cryostat (800 series

Cryostream Plus) attached to the diffractometer. The APEX III software was used for the unit cell determination and data collection.[20] Data reduction and global cell refinement were done using the Bruker SAINT software package[20] and the multi-scan, absorption correction was performed using SADABS.[21] The structure was solved using ShelXT,[22] by intrinsic phasing/direct methods, and refined with ShelXL,[23] by full-matrix least-squares on F^2, through the Olex2 interface program.[24] Non-hydrogen atoms were refined anisotropically. Hydrogen atoms were located in difference Fourier and refined using the riding model. The programs MERCURY[25] and ORTEP-3[26] were used to prepare the crystallographic information file (CIF) and artwork representations for publication. The CIF file was deposited in the Cambridge Structural Database under code 2005420.†

2.5. Measurement of $^1O_2$ photogeneration

The 1,3-diphenylisobenzofuran (DPBF) probe was used to measure the quantum yield of $^1O_2$ generation by the *cis*-[Fe(cyclam)Cl_2]Cl and [(Fe(cyclam))$_2$(Qz)]Cl$(PF_6)_3$ complexes and quinizarin ligand. DPBF is a fluorescent compound that reacts selectively with $^1O_2$ to produce a non-luminescent product. A series of 2.0 mL air-saturated methanol solutions containing DPBF (20 μmol L^{-1}) and the compounds were prepared in a 1 cm pathlength fluorescence cuvette and illuminated with LED light of 463 nm (Basetech Conrand, 1.7 W) for 100 s. The consumption of DPBF by its reaction with $^1O_2$ was followed by a decrease in fluorescence intensity at the emission maximum (λ_{ex} = 405 nm; λ_{em} = 449 nm) during different irradiation times. The quantum yield (Φ_Δ) for $^1O_2$ generation by the [Ru(bpy)$_3$]Cl_2 complex in air-saturated methanol, Φ_Δ = 0.87, was taken as a ref. 27. The $^1O_2$ generation quantum yield of the photosensitizers investigated the quinizarin ligand, *cis*-[Fe(cyclam)Cl_2]Cl and [(Fe(cyclam))$_2$(Qz)]Cl$(PF_6)_3$ complexes were determined according to eqn (1), where K is the slope of first order plots, K_s is related to the standard sensitizer (in our case, the [Ru(bpy)$_3$]Cl_2), and Φ_s is its $^1O_2$ quantum yield:[28,29]

$$\Phi_\Delta = \frac{K}{K_s}\Phi_s \quad (1)$$

2.6. Lipophilicity

The measurement of the log$P$ for the [(Fe(cyclam))$_2$(Qz)]Cl$(PF_6)_3$ complex was carried out following a modified procedure.[30] Briefly, *ca.* 0.5 mg of [(Fe (cyclam))$_2$(Qz)]Cl$(PF_6)_3$ complex was dissolved in 1 mL of octanol saturated water. Water saturated octanol (1 mL) was added and the mixture was shaken for 1 h in a thermo-mixer, at 28 °C at 1400 rpm. The samples were then subjected to centrifugation at 4300 rpm for 10 min to separate the aqueous from the organic phase. The lower phase (aqueous) was aspirated using a glass syringe. The organic phase was also collected and UV-vis absorption spectra were taken, and used to quantify the compound concentration in each phase. Previously, the molar absorptivity of the metal complexes was measured in both solvents and used in this quantification. log$P$ values were computed using the following formula: $\log P = \log(C_{octanol}/C_{water})$.

2.7. DNA cleavage assay

All measurements were carried out using an electrophoresis apparatus with agarose gel (0.8% w/v in TAE buffer, pH 8.0). The supercoiled pBR322 plasmid DNA was employed at 21 μmol L^{-1} in a nucleotide base pair, which was combined with the binuclear metal complex ([(Fe(cyclam))$_2$(Qz)]Cl$(PF_6)_3$), precursor metal complex ([Fe(cyclam)Cl_2]Cl) and free quinizarin. These samples were either exposed to blue light for 1 h, kept in the dark for 1 h or mixed with glutathione (10 mmol L^{-1}). In addition to these samples, a linear DNA ladder (1 kbp) was applied in the first lane of all gels. Plasmid DNA controls were also used either without any treatment (dark), irradiated with blue light or mixed with glutathione. A positive plasmid DNA control for light cleavage was employed using [Ru(bpy)$_3$]Cl_2 (at 30 μmol L^{-1}). After running the samples in agarose gel, it was stained with GelRed (1 mg mL^{-1}, Biotium) for 30 min, and the images were collected using a Gel Doc XR+ system (Biorad). All light irradiations were carried out using a Basetech Conrand, 1.7 W (λ_{max} = 463 nm) blue LED.

2.8 Cytotoxicity assays

Human lung adenocarcinoma (A549; CCL-185®), human prostate carcinoma (LNCaP clone FGC; CRL-1740™) and normal fibroblast (L929; CCL-1) cell lines from ATCC® (American Type Culture Collection, USA) were all purchased from the Rio de Janeiro Cell Bank (BCRJ). The cells were maintained in T-25 flasks containing DMEM medium (L929 and A549) or RPMI medium (LNCaP), both supplemented with 10% of fetal bovine serum (FBS), 1% of L-glutamine, 100 U mL^{-1} penicillin and 100 μg mL^{-1} streptomycin, at 37 °C, in a humidified atmosphere containing 5% CO_2. The culture medium was routinely changed every 3 days or when confluence reached *ca.* 85%, and then the cells were treated with trypsin (0.025% trypsin/0.1% EDTA) and subcultivated or used for the cytotoxicity assay.

2.8.1. *In vitro* cytotoxicity. In order to investigate the effect of quinizarin, *cis*-[Fe(cyclam)Cl_2]Cl and [(Fe(cyclam))$_2$(Qz)]Cl$(PF_6)_3$ on the cell viability, the MTS assay was carried out as previously described.[31] After trypsinization from T-25 flasks, cells (1.0×10^4/200 μL per well) were seeded in 96-well flat bottom plates. Different concentrations of the tested compounds (100–1.58 μg mL^{-1}) were dissolved in DMSO and then added to the wells. Afterwards, these plates were submitted to irradiation with a blue LED for 1 h and then incubated at 37 °C for 48 h in a 5% CO_2 incubator. Control or dark plates were prepared and incubated under the same conditions, but were not irradiated with the blue LED. After 48 h, all culture medium was removed and replaced with non-supplemented culture medium (DMEM or RPMI) containing MTS tetrazolium salt. An MTS assay was performed in all cell lines in which optical density was measured at 490 nm on a microplate reader (SpectraMax i3 Multi-Mode Microplate Reader). All assays were carried out in triplicate and also three independent experiments, where cell viability was calculated using eqn (2):

$$\text{Cell viability (\%)} = \frac{\overline{OD}_{490\,nm}(\text{compound})}{\overline{OD}_{490\,nm}(\text{control})} \times 100 \quad (2)$$

3 Results and discussion

The structure of $[(Fe(cyclam))_2(Qz)]Cl(PF_6)_3$ is shown in Fig. 1 and the crystallographic data and refinement parameters are given in Table 1.

The crystallographic data and selected bond lengths are shown in Tables 1 and 2, respectively.

The iron centers displayed a distorted octahedral geometry with the best equatorial planes defined by the oxygen atoms of the quinizarin and the nitrogen atoms from the cyclam ligand. It is important to note that the geometry around the iron atoms is very similar for both iron centers. Coordination of quinizarin to the iron centers induces the cyclam ligand to adopt a nonplanar configuration.

As can be seen from the structure of the metal complex (Fig. 1), the metal center forms a six-membered ring with a negative charge from the quinizarin ligand, dispersed over the π system. There is no full symmetry on both iron centers, further observed by the angles of O–Fe–O, which could be due to crystal asymmetric effects of counter-ions. Similar results of distances are found in the description of the crystal structure of the diiron complex $[Fe(salen)]_2Qz$.[14] The presence of one Cl^- and three PF_6^- ions disordered gives a charge balance consistent with a 4+ metal ion. Once the ligand is in the form of dihydroxyquinone anions doubly charged, it would require that both iron atoms are in the 3+ oxidation state.

The C–O distances of C1–O1 [1.320(8) Å], C4–O2 [1.317(8) Å], C6–O3 [1.285(7) Å], and C13–O4 [1.281(7) Å] for the 1,4-dioxido-9,10-anthraquinone bridging ligand in the X-ray structure of the metal complex are similar, but not equal. The fact that the keto forms of the C–O bonds are shorter than the enol ones suggests that there is not a total delocalization of the electrons in the rings involving the iron metal and the oxygens and the carbon atoms from the bridging ligand, as expected, for a not totally symmetrical structure. The correspondent values for these bonds are 1.352(4) Å, 1.351(4) Å, 1.236(3) Å and 1.237(4) Å, respectively, for the free ligand.[32] These data are also in agreement with low-spin species as reported for analogous iron metal complexes at low temperature.[33]

Table 1 Crystallographic data for refining the metal complex structure in the complex $[(Fe(cyclam))_2(Qz)]Cl(PF_6)_3$

Empirical formula	$C_{34}H_{54}ClF_{18}Fe_2N_8O_4P_3$
Molecular weight	1220.91
Crystalline system	Monoclinic
Space group	$P2_{1/c}$
Temperature (K)	150
Crystal size/mm^3	0.10 × 0.13 × 0.16
a (Å)	16.0603(5)
b (Å)	16.6212(6)
c (Å)	17.6984(7)
α (°)	90°
β (°)	92.069(2)°
γ (°)	90°
Volume/Å^3	4721.4(3)
Z	4
Absorption coefficient (mm^{-1})	7.501
$F(000)$	2488
Collected reflections	63 999
Independent reflections	8661 [R_{int} = 0.1206, R_{Sigma} = 0.0701]
F_2 fit quality	1.053
Final R indices [$I \geq 2\sigma(I)$]	R_1 = 0.0856, wR_2 = 0.2747
R indices (all data)	0.1316
CCDC	2005420

Table 2 Selected bond lengths [Å] and angles [°] for $[(Fe(cyclam))_2(Qz)]Cl(PF_6)_3$

Bond lengths (Å)		Bond angles (°)	
Fe1–O2	1.858(5)	O2 Fe1 O3	90.8(2)
Fe1–O3	1.905(4)	O2 Fe1 N1B	94.5(3)
Fe2–O1	1.859(5)	O2 Fe1 N5B	85.6(3)
Fe2–O4	1.910(5)	O2 Fe1 N8B	90.3(3)
Fe1–N1B	1.986(7)	O2 Fe1 N12B	177.4(3)
Fe1–N5B	2.009(7)	O3 Fe1 N1B	95.9(3)
Fe1–N8B	2.007(7)	O3 Fe1 N5B	176.1(3)
Fe1–N12B	2.005(7)	O3 Fe1 N8B	92.5(3)
Fe2–N1A	1.999(7)	O3 Fe1 N12B	86.7(2)
Fe2–N4A	2.004(6)	O1 Fe2 O4	91.2(2)
Fe2–N8A	1.972(6)	O1 Fe2 N1A	93.3(3)
Fe2–N11A	2.010(6)	O1 Fe2 N4A	177.5(2)
O2–C4	1.317(8)	O1 Fe2 N8A	90.0(3)
O1–C1	1.320(8)	O1 Fe2 N11A	85.3(2)
O3–C6	1.285(7)	O4 Fe2 N1A	89.9(2)
O4–C13	1.281(7)	O4 Fe2 N4A	87.1(2)
		O4 Fe2 N8A	93.9(2)

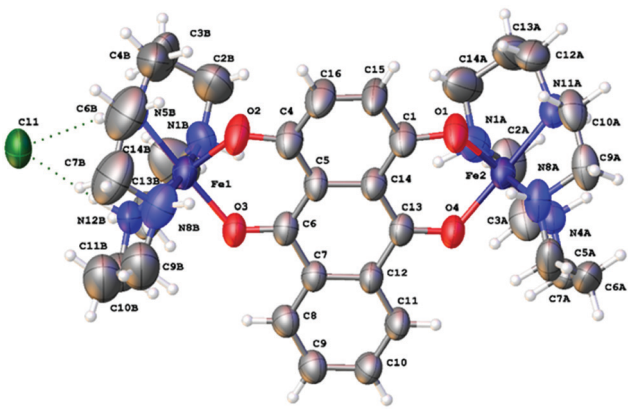

Fig. 1 ORTEP view of the $[(Fe(cyclam))_2(Qz)]Cl^{3+}$ cation complex, showing labeling and 50% probability ellipsoids. Three PF_6^- ions were omitted for the sake of clarity.

As can be seen from the above data, the C–O bonds in the enol forms, in the free ligand, after its coordination to the iron metal were shortened, while the bonds in the keto forms were increased. This behavior shows the occurrence of electron resonance in the coordinated bridging ligand. A similar pattern was observed for the ruthenium complexes $[Ru(Lap)(dppm)_2]PF_6$ and $[Ru(Law)(dppm)_2]PF_6$, where dppm = 1,1′-bis(diphenylphosphino)methane, and Lap and Law are naphthoquinones, lapachol and lawsone, respectively.[34] It is also worth pointing out that the lengths of the Fe–O bonds (see Table 2) are very close for both oxygen atoms, confirming the suggestion of resonance in the 1,4-dihydroxyantraquinone coordinated ligand.

The vibrational spectrum of the metal complex in the infrared region also corroborates the proposal for the determination of the coordination mode of the Qz ligand to the metal

centers. The carbonyl functional groups of the Qz involved in the coordination of the ligand with the metal center were studied, which showed changes in the spectrum of the diiron complex, if compared with the spectrum of the free ligand (Fig. S1, ESI†). There is no broad band at *ca.* 3354 cm^{-1} assigned to ν(OH) vibration, indicating the deprotonation of this group and supporting its coordination to the iron atom. In addition to that, the spectrum of the iron complex showed a shift of *ca.* 5 cm^{-1} of the coordinated carbonyl groups if compared with the frequencies of the free Qz ligand, indicating a bidentate coordination mode of these groups to the iron center. In the free Qz, the bands of the stretching mode of C4–O2 and C1–O1 were observed at 1630 cm^{-1}, while the C6–O3 and C13–O4 are at 1590 cm^{-1}. Furthermore, the bands around 840 cm^{-1} and 558 cm^{-1} are attributed to ν(P–F) and δ(P–F) stretching vibration modes, indicating the presence of a counterion PF_6^- in the complex. These results supported that the bridged ligand is bound to the two iron ions *via* the oxygens of the carbonyl groups.

Vibrational bands characteristic of νCH and νCN stretching modes of the cyclam ligand[35] were also observed in the range of 1460–1430 cm^1 along with the band at 1532 cm^{-1}, which probably belongs to the aromatic rings' breathing mode.[36]

The binuclear compound was further analyzed by Mössbauer spectroscopy and compared with the precursor metal complex, *cis*-[Fe(cyclam)Cl_2]Cl. Fig. 2 shows the Mössbauer spectra of the precursor complex *cis*-[Fe(cyclam)Cl_2]Cl and the binuclear complex [(Fe(cyclam))$_2$(Qz)]Cl$(PF_6)_3$ at 298 K. The hyperfine parameters are shown in Table 3, where the isomer shift (δ) can be used to determine the oxidation state of the metal, while the quadrupole splitting (Δ) is a rough measurement of the charge distribution around the metal site.

The Mössbauer spectrum of the precursor complex (Fig. 2a) showed only a singlet signal with an isomer shift of 0.32 mm s^{-1}. According to magnetic susceptibility and EPR experiments,[19,37] the *cis*-[Fe(cyclam)Cl_2]Cl complex presents a high spin configuration, which in an octahedral microsymmetry, gives rise to the distribution $(t_{2g})^3(e_g)^2$. These electrons are evenly distributed in the orbitals, thus originating the singlet signal noticed in the Mössbauer spectrum. It is important to note that the *trans*-[Fe(cyclam)Cl_2]Cl showed a doublet signal with the quadrupolar splitting of 2.50 mm s^{-1} (Table 3), which can be explained by its low-spin configuration $(t_{2g})^5$ with asymmetric charge distribution in the orbitals. Indeed, *trans*-[Fe(cyclam)Cl_2]Cl is a low-spin complex as shown in the literature.[19,37] These results support the dominant effect of electron distribution *versus* structural symmetry on the quadrupolar splitting. Otherwise, the best fit to the Mössbauer spectrum of the [(Fe(cyclam))$_2$Qz]Cl$(PF_6)_3$ complex (Fig. 2b) was achieved using two doublets, typical for two types of iron centers as measured. Isomer shift and quadrupole splitting values are consistent with Fe^{3+} in octahedral sites. The doublets have very different quadrupole splitting values. Moreover, the relative areas under the subspectra suggest a near equal distribution of iron ions in each environment. These results cannot be explained by the modest structural asymmetry of the iron centers as indicated by X-ray analysis, but are indicative of an equilibrium of populations containing high- and low-spin iron centers. The wide doublet (green line) is consistent with a low spin configuration and the narrow doublet (blue line) is typical of the high spin configuration.[38,39] This measurement was carried out at 298 K, which might allow a mixture of these configurations. At lower temperature it might favor low-spin species, which is in agreement with X-ray measurements taken at 150 K.[33]

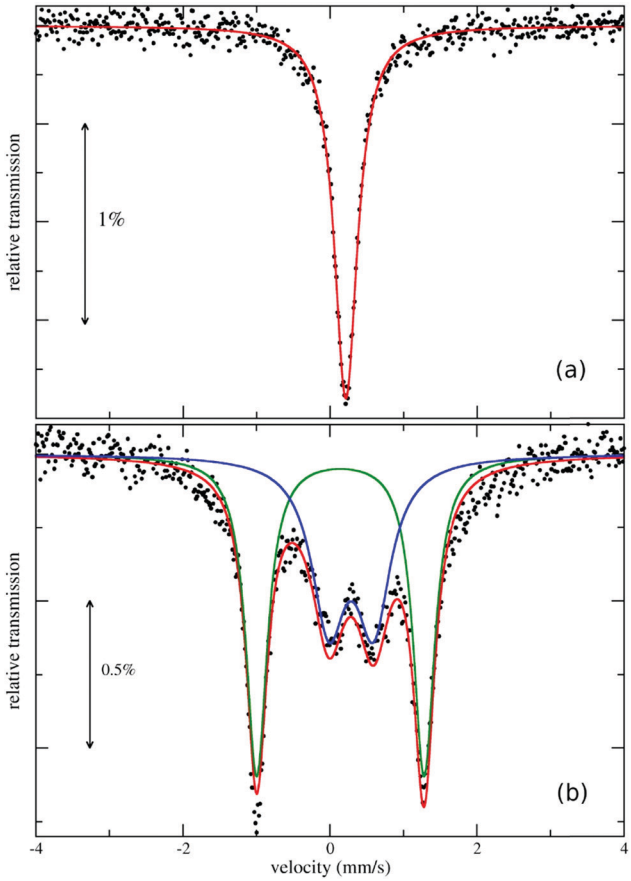

Fig. 2 Mössbauer spectra of the precursor complex *cis*-[Fe(cyclam)Cl_2]Cl (a) and the binuclear complex [(Fe(cyclam))$_2$Qz]Cl$(PF_6)_3$ (b). For spectrum b: black dots: experimental data; green and blue lines: subspectra of Fe^{3+} in octahedral sites; red line: best fit to the data, sum of green and blue lines.

Previously, Poon *et al.* showed by EPR that *trans*-[Fe(cyclam)Br_2]ClO_4 exhibited a temperature-dependent spin transition from low- to high-spin configuration.[36] More recently, other cyclam-based iron complexes also showed this behavior called spin crossover, whose transition can even occur at room temperature.[38,40] This interesting phenomenon has been widely reported in many metal complexes including catecholate-based ones, where a low to high-spin configuration can be modulated by temperature, pressure and more rarely, by light.[39] This process can find many interesting applications on molecular switching devices (*e.g.*, sensors, memory display devices, *etc.*). The [(Fe(cyclam))$_2$(Qz)]Cl$(PF_6)_3$ complex showed features consistent with a spin crossover process, including Mössbauer data and bonding distances at low temperature consistent with a low-spin state.[39] Nevertheless, this interesting property must be further investigated to reveal its potential.

Table 3 Hyperfine parameters of Mössbauer spectra of the precursor complex *cis*-[Fe(cyclam)Cl_2]Cl (a) and of the binuclear complex [(Fe(cyclam))$_2$(Qz)]Cl$(PF_6)_3$. Uncertainties smaller than 0.1 mm s^{-1} (δ, Δ, Γ) and 1% (area) (at 298 K)

Sample	Subspectrum	δ (mm s^{-1})	Δ (mm s^{-1})	Γ (mm s^{-1})	Area (%)
cis-[Fe(cyclam)Cl_2]Cl	Singlet	0.32	—	0.38	100
[(Fe(cyclam))$_2$Qz]Cl$(PF_6)_3$	Doublet 1 (blue)	0.40	0.61	0.56	45
	Doublet 2 (green)	0.25	2.28	0.35	55
trans-[Fe(cyclam)Cl_2]Cl	Doublet	0.25	2.50		100
Sr_3[Fe(ox)$_3$]	Doublet	0.29	0.40		100

In order to examine the electrochemical properties of the new binuclear iron complex, cyclic voltammetric (CV) measurements were carried out in the voltage range of −1.0 to 1.0 V. This cyclic voltammogram is shown in Fig. 3b. Previously, the literature reported the redox activity of the quinizarin ligand in dimethylformamide, which led us to acquire a new CV in acetonitrile (Fig. 3a) for the sake of comparison. The cyclic voltammogram of the free Qz showed two redox waves, which can be considered reversible processes, with potentials that agreed with previously reported values at different solvents, at $E_{1/2}$ = −0.646 V and $E_{1/2}$ = −1.123 V assigned from the quinone (Qz^{2-}) to semiquinone (Qz^{3-}) and from the semiquinone (Qz^{3-}) to catechol (Qz^{4-}) processes, respectively, as shown in Scheme 1.[41]

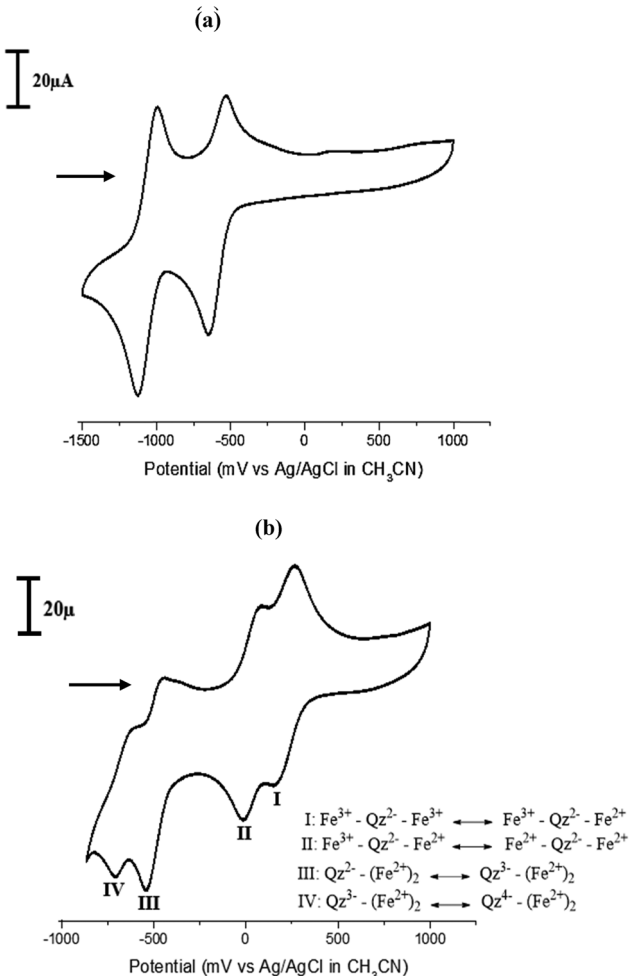

Fig. 3 Cyclic voltammograms of (a) the free quinizarin ligand and (b) the [(Fe(cyclam))$_2$(Qz)]Cl$(PF_6)_3$ complex in CH_3CN/0.1 M Et_4NClO_4 *versus* Ag/AgCl, scan rate 50 mV s^{-1}.

It is also important to mention that both moieties of the diiron complex, either metal ions and the bridging ligand Qz, are capable of undergoing at least a total of three reversible one-electron transfer processes at variable potentials. First of all, two redox waves at −0.538 (III) and −0.728 V (IV) were observed for the metal complex, which were nearly in the same range of redox potential of the free quinizarin molecule. This observation suggests that these redox processes involve the coordinated quinone/semiquinone ($Qz^{2-}(Fe^{2+})_2$)/($Qz^{3-}(Fe^{2+})_2$) and semiquinone/catechol ($Qz^{3-}(Fe^{2+})_2$)/($Qz^{4-}(Fe^{2+})_2$). The redox potentials of the coordinated quinizarin ligand were significantly shifted toward the anodic direction, relative to values observed for the free Qz. This behavior can be explained by considering that the coordination of quinizarin with the iron centers may cause a movement of the electronic density from the ligand toward the metal center, which withdraws the electron density out from the ligand. Consequently, this species becomes more susceptible to undergo a reduction process, at less negative potentials. It is also important to mention that, in negative potential, both metal centers are in the reduced form (Fe^{2+}). Besides the waves associated to the ligand at low potential, two extra reversible redox processes are also observed in the voltammogram of the binuclear complex in the potential range from 0.0 to 1.0 V. These higher potential waves are attributed to the redox processes centered at the metal centers.

The first oxidation process at 0.159 V can be assigned to the formation of a mixed-valence complex Fe^{3+}–Qz^{2-}–Fe^{2+}, followed by a second oxidation process at 0.250 V, Fe^{3+}–Qz^{2-}–Fe^{3+}. The corresponding reduction processes of these species are at 0.017 V and 0.200 V, respectively. This behavior may be due to a great electronic coupling between the iron centers, which without communication should exhibit only one single electrochemical potential for $Fe^{3+/2+}$. These two metal-based redox processes can be used to calculate the comproportionation constant (K_c) for this system ($\log K_c$) = 16.9 ($E_{1/2}{}^1 - E_{1/2}{}^2$ at 25 °C),[42,43] which provides

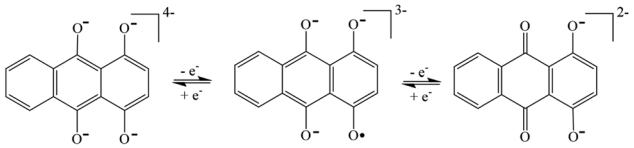

Scheme 1 Electrochemical processes associated with the quinizarin molecule.

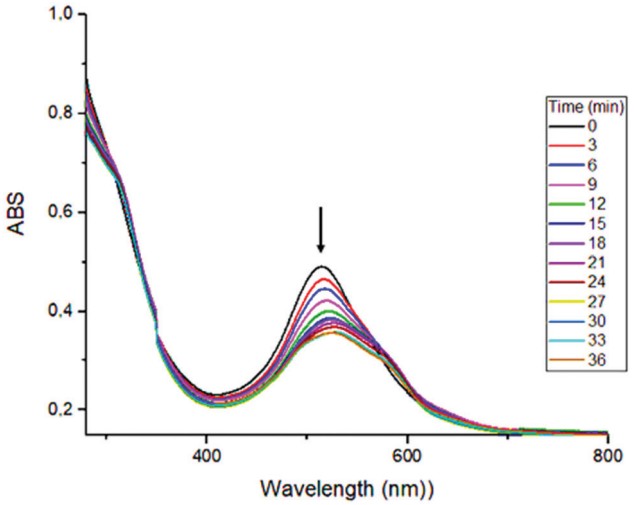

Fig. 4 UV/Vis/NIR spectroelectrochemical response of $[(Fe(cyclam))_2(Qz)]Cl(PF_6)_3$ on the reduction applying a negative potential (−1.0 V) for 36 minutes in CH_3CN/0.1 M Bu_4NPF_6.

information of the extent of electron delocalization between the iron centers. This binuclear metal complex showed a K_c of 943, which is significantly higher, even if compared to other binuclear iron complexes such as the one bridged by pyrazine (K_c = 50).[44]

The redox processes of the metal complex were also investigated *via* UV/vis/NIR spectroelectrochemistry in acetonitrile to establish the likely sites of electron transfer. First of all, it is important to mention that no intervalence charge transfer (IVCT) bands for the $[(Fe(cyclam))_2Qz]Cl(PF_6)_3$ complex were observed in the near-infrared region searched (Fig. S2, ESI†), indicating that the oxidation states of both metal sites are likely in the Fe(III)–Fe(III). This result corroborates with the single-crystal X-ray and Mössbauer analysis. Spectroelectrochemical measurements in the UV-vis region were also carried out and spectroscopic changes are shown in Fig. 4 and Fig. S3 (ESI†). We observed that when applying a positive potential (+1000 mV) there was no change in the UV-vis spectrum (Fig. S3, ESI†). This result indicated that both species (Qz ligand and metal centers) were already in the completely oxidized state ($Qz^{2-}(Fe^{3+})_2$). On the other hand, by applying a negative potential (−1000 mV) for *ca.* 36 minutes, an intense ligand-to-metal charge transfer (LMCT $d\pi Fe^{III} \leftarrow \pi^*$ (Qz)) band at 517 nm diminished by almost half of its intensity, suggesting the formation of the completely reduced species ($Qz^{4-}(Fe^{2+})_2$). Nonetheless, all results collected supported a formulation of $[(Fe(cyclam))_2Qz]Cl(PF_6)_3$ for this compound.

3.1. Photoproduction of $^1O_2$

It is important to mention that singlet oxygen has been considered as a major cytotoxic and genotoxic species to eukaryotic cells, bacteria and viruses. Moreover, $^1O_2$ has been implicated in the induction of tumours by photosensitizations and in the metabolic activation of carcinogens.[45,46] In this context, $^1O_2$ may also be responsible for the side effects of anthracycline drugs. Based on that, we decided to study the potential photogeneration of reactive oxygen species induced by the compounds described herein. Initially, we measured the quantum yield for $^1O_2$ generation (Φ_Δ) by the $[(Fe(cyclam))_2(Qz)]Cl(PF_6)_3$, *cis*-$[Fe(cyclam)Cl_2]Cl$ and quinizarin ligand. This study was performed by monitoring the reaction of $^1O_2$ with DPBF, an efficient $^1O_2$ scavenger.[28,29] The consumption of DPBF in a methanol solution was monitored by its emission intensity decreasing at 449 nm. As shown in Fig. S4 (ESI†), the plots of $\ln(I_t/I_0)$ as a function of the irradiation time are roughly linear for all species tested (I_0 and I_t are the fluorescence intensities of DPBF before and after irradiation, respectively). For the sake of comparison, the Φ_Δ of the classic singlet oxygen photogenerator $[Ru(bpy)_3]Cl_2$ was measured under the same conditions. The values of Φ_Δ were calculated using the linear regression data from Fig. S4 (ESI†) and eqn (1), employing $[Ru(bpy)_3]Cl_2$ as the standard (Φ_Δ =0.87).[27] The $^1O_2$ quantum yields for the $[(Fe(cyclam))_2Qz]Cl(PF_6)_3$ complex were found at *ca.* 0.130, whereas the precursor complex, *cis*-$[Fe(cyclam)Cl_2]$, did not show any significant production. Interestingly, the quinizarin ligand exhibited quantum yield at 0.122, very close to the binuclear complex, but still much lower than $[Ru(bpy)_3]Cl_2$ (0.87). This study was also carried out without light irradiation, where there was no change in DPBF fluorescence discarding also any fluorescence quenching. Furthermore, there was also no decomposition of the binuclear metal complex upon blue light irradiation as indicated by the lack of changes in the UV-vis spectrum under these conditions. These results show that the $[(Fe(cyclam))_2(Qz)]Cl(PF_6)_3$ complex has an apparent capacity for $^1O_2$-generation. This process might be important as it can more easily promote DNA photocleavage and cause other biological effects, which was further explored.

3.2 DNA cleavage

The generation of reactive oxygen species (ROS) by quinizarin itself or bound to a metal ion might have important implications, considering that this ligand is a model for the dihydroxyquinone moiety found in anthracycline drugs. The literature reports that the cardiotoxicity of anthracyclines involves the coordination of iron. This potential metal complex of iron-anthracycline might function as a catalyst generating ROS (*e.g.*, $OH^\bullet$, O_2^{-}).[11] These species could account for the cardiotoxicity and cytotoxic effects of these drugs involving damage to DNA, proteins and cell membranes. Some quinone-based compounds have also shown the capacity to generate superoxide or hydrogen peroxide upon the action of a reducing agent (*e.g.*, glutathione, GSH), which could also help to damage cells.[47] Notably, glutathione is a thiol-based compound found in significantly high concentrations in cells (up to 10 mmol L^{-1}) functioning as a redox buffering agent.[48] Despite the fact that glutathione works as an antioxidant agent, it can also paradoxically function to generate more reactive species (*e.g.*, O_2^{-}) through metal compound assistance. Indeed, there are many metallocompounds that can consume oxygen and reduce glutathione (or ascorbic acid) to generate ROS also known as catalytic metallodrugs. This can cause not only a drop in the

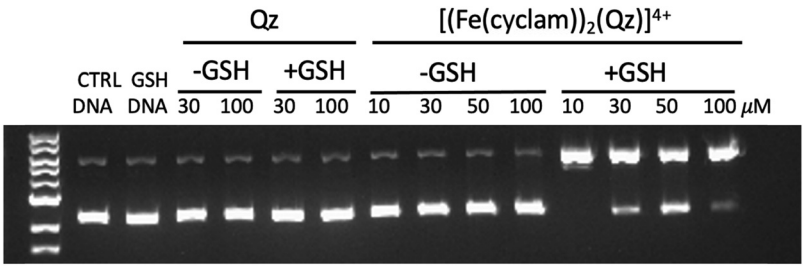

Fig. 5 DNA cleavage assay using glutathione at 10 mmol L^{-1} with quinizarin (Qz) and binuclear metal complex ($[(Fe(cyclam))_2(Qz)]^{4+}$) at variable concentrations. Note that "−GSH" and "+GSH" means without and with glutathione added, respectively.

cytosolic levels of glutathione but a rise in oxidizing species able to damage macromolecules. Indeed, ROS can usually cause damage to DNA by oxidizing guanine and abstracting hydrogen from ribose leading to DNA strand scission.[49]

First of all, we decided to investigate if any DNA damage could occur as a consequence of blue light irradiation, once we observed a modest production of singlet oxygen. If the DNA was damaged using light with the binuclear complex, then it might open up opportunities for phototherapeutical studies. Thus, in this experiment we used $[(Fe(cyclam))_2(Qz)]Cl(PF_6)_3$, *cis*-$[Fe(cyclam)Cl_2]Cl$ and quinizarin ligand, which were incubated with pBR322 plasmid DNA, and kept for 1 h in the dark or irradiated with blue light, before running in an agarose gel. The $[Ru(bpy)_3]Cl_2$ complex (TBP), a known singlet oxygen photogenerator, was also used as a positive control for DNA photocleavage, under the same conditions. However, this experiment did not show any significant evidence of DNA cleavage under such conditions (Fig. S5, ESI†), indicating that neither thermal nor blue light might be enough to cause damage to the DNA. Therefore, other studies using light were not further promoted.

Aiming at the investigation of other potential routes of ROS generation, we also studied the effect of reducing agents, particularly glutathione, in the binuclear complex. Indeed, glutathione was chosen considering that cells have plenty of this molecule, but also due to its function as a substrate for catalytic reduction of oxygen originating ROS.[47,50] In this study, we mixed glutathione with the binuclear metal complex or free quinizarin in the presence of DNA, which was incubated for 1 h in the dark. The quinizarin ligand did not promote any significant changes in the DNA, despite the fact that its redox quinone-catechol behavior could eventually originate ROS species. On the other hand, the binuclear metal complex showed a remarkable capacity to cleave DNA when adding glutathione. Even at 10 μmol L^{-1} of $[(Fe(cyclam))_2(Qz)]Cl(PF_6)_3$, we observed a major conversion of supercoiled DNA (form I) into nicked DNA (form II, single strand DNA cleavage) (Fig. 5). This behavior might be explained considering the redox potential of glutathione at *ca.* −504 mV (in an aqueous buffer pH 8.0), which might not be able to reduce free quinizarin ($E_{1/2}$ = −646 mV, in acetonitrile); therefore, this ligand cannot catalytically generate ROS (Fig. 5). However, this reducing agent can fully reduce the iron center of the binuclear complex ($E_{1/2}$ = +159 mV and −17 mV in acetonitrile) and might convert the bound quinizarin ligand from quinone to semiquinone species ($E_{1/2}$ = −538 mV in acetonitrile). This process of chemical reduction and eventual reoxidation by oxygen might generate ROS species enabling DNA damage. This type of process has been reported for other quinone-catechol-based compounds and iron or copper complexes.[47,50–53]

To investigate the likely identity of the deleterious species involved in the DNA damage, we setup a new experiment mixing $[(Fe(cyclam))_2(Qz)]Cl(PF_6)_3$, DNA and glutathione, but also including four selective ROS scavenger agents (Fig. 6). These agents were chosen based on their ability to suppress $^1O_2$ (sodium azide), $^{\bullet}OH$ (mannitol), H_2O_2 (sodium pyruvate) and $O_2^{\bullet-}$ (4,5-dihydroxy-1,3-benzenedisulfonic acid, tiron), as reported in the literature.[54,55] Interestingly, the binuclear complex (1 in the gel, Fig. 6) showed efficient cleavage of DNA, which was strongly suppressed when adding sodium pyruvate and tiron.

This behavior indicates that the reaction of the $[(Fe(cyclam))_2(Qz)]Cl(PF_6)_3$ with glutathione may generate superoxide and hydrogen peroxide as the main species involved in DNA cleavage (Fig. 7).

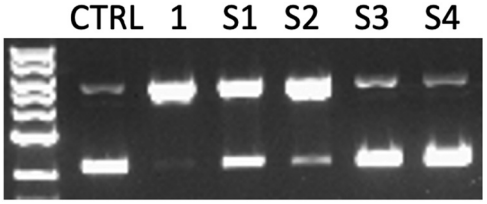

Fig. 6 Investigation of ROS involved in DNA cleavage mediated by the binuclear complex. The CTRL lane contains only DNA while all other lanes contain DNA, 50 μmol L^{-1} of $[(Fe(cyclam))_2(Qz)]Cl(PF_6)_3$ and 10 mmol L^{-1} of glutathione. The following suppressors were added at 30 mmol L^{-1} in: S1 (sodium azide), S2 (mannitol), S3 (sodium pyruvate) and S4 (tiron).

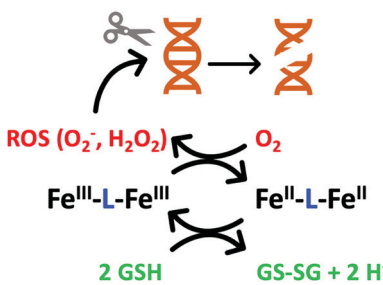

Fig. 7 Proposal of the DNA damage led by the binuclear complex upon reduction.

These interesting results are in line with the well-known behavior of ROS generated in cells, which can lead to impaired physiological function through cellular damage of DNA, proteins, lipids, and other macromolecules. It can also lead to certain human pathologies including cancer, neurodegenerative disorders, and cardiovascular diseases, as well as aging,[56] and therefore a balance between the harmful and beneficial action of ROS is essential to prevent toxicity.

3.3 Lipophilicity

The fate of a drug in the body is very complex, but some early properties can indicate better chances of success. Among these properties, the solvent partition of a compound as measured by the log *P* is an important hint. This value may reflect the hydrophilicity/lipophilicity of a compound and can suggest its capacity to cross cell membranes. Our measurement of log *P* for the binuclear complex $[(Fe(cyclam))_2(Qz)]Cl(PF_6)_3$ was carried out, where a value of 0.42 was obtained. This moderately low log *P* is still in a lipophilic range and might support its potential to cross membranes. Nonetheless, we must be aware that many other features can define the fate of a compound, including its overall charge, which in our case is significantly high (4+).

3.4 Anticancer activity

Aiming to evaluate the potential role of the binuclear complex against cancer and normal cells, the effect of $[(Fe(cyclam))_2(Qz)]Cl(PF_6)_3$ on the viability of two cancer cell lines, LNCaP (prostate cancer) and A549 (lung cancer), and one normal cell line, L929 (mouse fibroblast), was determined using an MTS assay (Fig. 8). These cells were treated with various concentrations of $[(Fe(cyclam))_2(Qz)]Cl(PF_6)_3$ (1.58, 3.12, 6.25, 12.5, 25.0, 50.0 and 100.0 μg mL^{-1}) for 48 h in the presence or absence of light

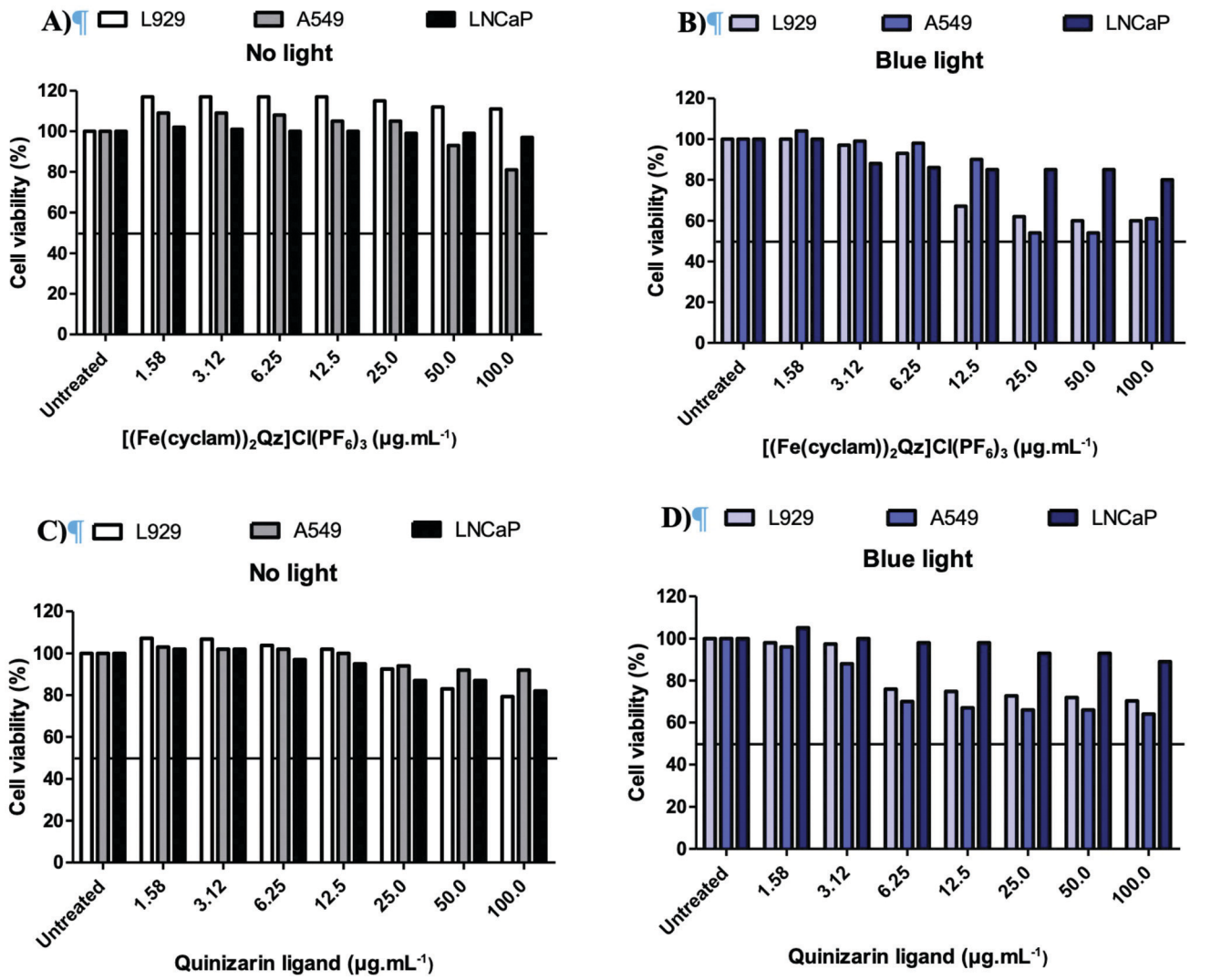

Fig. 8 $[(Fe(cyclam))_2(Qz)]Cl(PF_6)_3$ and free quinizarin reduce the viability of A549 and L929 cell lines just after irradiation with a blue LED (λ_{irr} = 453 nm). The viability of cells treated with increasing concentrations of $[(Fe(cyclam))_2(Qz)]Cl(PF_6)_3$ (without and with blue light, A and B, respectively) and free quinizarin (without and with blue light, C and D, respectively) (1.58, 3.12, 6.25, 12.5, 25.0, 50.0 and 100.0 μg mL^{-1}) for 48 h were obtained by normalizing the absorbance measured in each case over those of its respective untreated control. Bar graphs represent the means (±SD) of triplicates of three independent measurements.

(λ_{irr} = 453 nm). The same experiment was also carried out for the *cis*-[Fe(cyclam)Cl_2]Cl complex and for the free quinizarin ligand. In the case of the *cis*-[Fe(cyclam)Cl_2]Cl complex, there was no effective inhibition of cell viability, even at high concentrations and after light irradiation (Fig. S6, ESI†). However, there was a mild reduction in cell viability of A549 and L929 cells starting at 6.25 μg mL^{-1} and 12.5 μg mL^{-1} for the quinizarin ligand and [(Fe(cyclam))$_2$(Qz)]Cl$(PF_6)_3$, respectively, if compared with the control group, which was only observed with light irradiation (Fig. 8). The cytotoxic effect was more effective for the binuclear compound at higher concentrations. It is important to note that the binuclear complex and free quinizarin minimally affected malignant cells and also normal cells after light irradiation, indicating low selectivity for tumor cells. Nonetheless, it is worth mentioning that the low cytotoxicity of the binuclear complex was somewhat of a surprise, considering that this compound showed a high capacity to cleave DNA, in the presence of a reducing agent in particular. However, we must also consider other issues on a complex cellular medium, including its cellular uptake.[57] This compound may have intracellular targets (such as DNA); therefore, it must penetrate the lipid bilayer of cellular membranes to reach them. Therefore, its moderately low lipophilicity indicated by the log*P* and unknown uptake might hinder its cytotoxic activity. These features could be further investigated and altered as a strategy to improve biological activity.

4 Conclusions

The comproportionation constant found for the binuclear Fe^{3+} complex, containing the quinizarin as the bridging ligand, is high, showing strong electron delocalization between the iron centers.[42,43] The binuclear complex showed a high capacity to damage DNA in the presence of a biological reducing agent, a property that is not observed for the free quinizarin ligand. The shift of the redox potential for quinizarin upon binding to iron can be responsible for that process, where superoxide and hydrogen peroxide may be produced causing DNA cleavage. Although the binuclear compound exhibited a high capacity to damage the DNA, its cytotoxicity was still very low. This might be due to a low lipophilicity of the complex [(Fe(cyclam))$_2$(Qz)]Cl$(PF_6)_3$, preventing a better uptake, which is under investigation. Nevertheless, the promising chemical properties of this compound as the ROS generator can still be further explored as a potential drug by designing modifications to improve hydrophobicity and or using a delivery platform to achieve cell targets.[31,58,59]

In this work, we showed that a mimic of the anthracycline drug, upon binding to iron, can produce deleterious molecules, which might be associated with multiple undesired side effects caused by this type of compound.

Conflicts of interest

There are no conflicts to declare.

Acknowledgements

We are thankful to CNPq (E. H. S. Sousa 308383/2018-4, Universal 403866/2016-2) CAPES/PROEX (23038.000509/2020-82 – PROEX program – 1227/2020) for the financial support. This study was also financed in part by the Coordenação de Aperfeiçoamento de Pessoal de Nível Superior – Brasil (CAPES) – Finance Code 001.

References

1 D. Agudelo, P. Bourassa, G. Bérubé and H. A. Tajmir-Riahi, *J. Photochem. Photobiol., B*, 2016, **158**, 274–279.
2 P. Ma and R. J. Mumper, *Nano Today*, 2013, **8**, 313–331.
3 C. Carvalho, R. Santos and S. Cardoso, *Curr. Med. Chem.*, 2009, **16**, 3267–3285.
4 G. Minotti, P. Menna, E. Salvatorelli, G. Cairo and L. Gianni, *Pharmacol. Rev.*, 2004, **56**, 185–229.
5 S. Jasra and J. Anampa, *Curr. Treat. Options Oncol.*, 2018, **19**, 1–17.
6 O. Tacar, P. Sriamornsak and C. R. Dass, *J. Pharm. Pharmacol.*, 2013, **65**, 157–170.
7 Y. Fujun, D. Jing, W. Ying, Z. Yue, G. Yanli, G. Huilin and K. Xiaofeng, *Anal. Chem.*, 2015, **87**, 338–342.
8 M. B. Martins-Teixeira and I. Carvalho, *ChemMedChem*, 2020, **15**, 933–948.
9 K. Chatterjee, J. Zhang, N. Honbo and J. S. Karliner, *Cardiology*, 2010, **115**, 155–162.
10 E. J. F. Demant, *FEBS Lett.*, 1984, **176**, 97–100.
11 S. Zhang, X. Liu and T. Bawa-Khalfe, *Nat. Med.*, 2012, **18**, 1639–1642.
12 S. Rawat, A. Jaiswal, A. Khurana and S. Bhatti, *Biomed. Pharmacother.*, 2021, **139**, 111708.
13 R. Kiraly and R. B. Martin, *Inorg. Chim. Acta*, 1982, **67**, 13–18.
14 M. J. Maroney, R. O. Day, T. Psyris, L. M. Fleury and J. P. Whitehead, *Inorg. Chem.*, 1989, **28**, 173–175.
15 S. Maji, B. Sarkar and S. M. Mobin, *Inorg. Chem.*, 2008, **47**, 5204–5211.
16 A. Mandal, A. Grupp, B. Schwederski, W. Kaim and G. K. Lahiri, *Inorg. Chem.*, 2015, **54**, 7936–7944.
17 M. Kozsup, O. Dömötör, S. Nagy, E. Farkas, E. A. Enyed and P. Buglyó, *J. Inorg. Biochem.*, 2020, **204**, 110963.
18 S. Füzerová, J. Kotek, I. Císařová, P. Hermann, K. Binnemansa and I. Lukeš, *Dalton Trans.*, 2005, **17**, 2908–2915.
19 R. Guilard, O. Siri and A. Tabard, *J. Chem. Soc., Dalton Trans.*, 1997, **19**, 3459–3463.
20 Bruker AXS Inc. APEXIII. Version 2016-1, 2018.
21 G. M. Sheldrick, SADABS. Version 2008-1, 2008.
22 G. M. Sheldrick, *Acta Crystallogr., Sect. A: Found. Crystallogr.*, 2015, **71**, 3–8.
23 G. M. Sheldrick, *Acta Crystallogr., Sect. C: Struct. Chem.*, 2015, **71**, 3–8.
24 O. V. Dolomanov, L. J. Bourhis, R. J. Gildea, J. A. K. Howard and H. Puschmann, *J. Appl. Crystallogr.*, 2009, **42**, 339–341.

25 C. F. Macrae, P. R. Edgington, R. McCabe, E. Pidcock, R. Taylor and M. Towler, *J. Appl. Crystallogr.*, 2006, **39**, 453–457.
26 L. Farrugia, *J. Appl. Crystallogr.*, 1997, **30**, 565.
27 C. Tanielian, C. Wolff and M. Esch, *J. Phys. Chem.*, 1996, **100**, 6555–6560.
28 F. D. Abreu, T. D. F. Paulo, M. H. Gehlen, R. A. Ando, L. G. F. Lopes, A. C. S. Gondim, M. A. Vasconcelos, E. H. Teixeira, E. H. S. Sousa and I. M. M. Carvalho, *Inorg. Chem.*, 2017, **56**, 9084–9096.
29 H. Y. Ding, X. S. Wang and L. Q. Song, *J. Photochem. Photobiol., A*, 2006, **177**, 286–294.
30 C. Al Hageh, M. Al Assaad and Z. El Masri, *Dalton Trans.*, 2018, **47**, 4959–4967.
31 G. F. Oliveira, F. S. Gouveia Jr, A. A. Pinheiro, L. G. N. Neto, M. A. Vasconcelos, E. H. Teixeira, A. C. S. Gondim, L. G. F. Lopes, I. M. M. Carvalho and E. H. S. Sousa, *New J. Chem.*, 2020, **44**, 6610–6622.
32 G. D. Nigam and B. Deppisch, *Z. Kristallogr.*, 1980, **151**, 185–191.
33 C. Eric, B. Marie-Laure, H. Johan, M. Nicolas, S. Marina, L. Maciej, T. Loïc, B. Marylise, T. Antoine and J. Sainton, *Acta Crystallogr., Sect. B: Struct. Sci.*, 2009, **65**, 474–480.
34 K. Oliveira, J. Honorato, F. Demidoff, M. S. Schultz, C. D. Netto, M. R. Cominetti and R. S. Correa, *J. Inorg. Biochem.*, 2021, **214**, 111289.
35 A. K. M. Holanda, F. O. N. Silva, I. M. M. Carvalho, A. A. Batista, J. Ellena, E. E. Castellano, I. S. Moreira and L. G. F. Lopes, *Polyhedron*, 2007, **26**, 4653–4658.
36 P. H. Merrell, *Inorg. Chim. Acta*, 1979, **32**, 99–102.
37 P. K. Chan and C. K. Poon, *J. Chem. Soc., Dalton Trans.*, 1975, **858**, 858–862.
38 P. J. V. Koningsbruggen, Y. Maeda and H. Oshio, Iron(III) Spin Crossover Compounds. In: Spin Crossover in Transition Metal Compounds I, *Top. Curr. Chem.*, 2004, 259–324.
39 D. J. Harding, P. Harding and W. Phonsri, *Coord. Chem. Rev.*, 2016, **313**, 38–61.
40 B. Drahoš and Z. Trávníček, *Dalton Trans.*, 2018, **47**, 6134–6145.
41 A. Ashnagar, J. M. Bruce, P. L. Dutton and R. C. Prince, *Biochim. Biophys. Acta, Gen. Subj.*, 1984, **801**, 351–359.
42 D. E. Richardson and H. Taube, *Inorg. Chem.*, 1981, **20**, 1278–1285.
43 D. E. Richardson and H. Taube, *Coord. Chem. Rev.*, 1984, **60**, 107–129.
44 F. Felix and A. Ludi, *Inorg. Chem.*, 1978, **17**, 1782–1784.
45 S. Callaghan and M. O. Senge, *Photochem. Photobiol. Sci.*, 2018, **17**, 1490–1514.
46 P. R. Ogilby, *Chem. Soc. Rev.*, 2010, **39**, 3181–3209.
47 S. Kim, J. H. Seo and D. I. Jeong, *Biomater. Sci.*, 2021, **9**, 847–860.
48 D. P. Jones, *Methods Enzymol.*, 2002, **348**, 93–112.
49 W. K. Pogozelski and T. D. Tullius, *Chem. Rev.*, 1998, **98**, 1089–1107.
50 W. M. Medeiros, M. J. Medeiros and E. M. Carvalho, *RSC Adv.*, 2018, **8**, 16873–16886.
51 H. Liu, X. Qu and E. Kim, *Biomaterials*, 2018, **162**, 109–122.
52 D. R. A. Mans, M. V. M. Lafleur, E. J. Westmijze, I. R. Horn, D. Bet, G. J. Schuurhuis, J. Lankelma and J. Retel, *Biochem. Pharmacol.*, 1992, **43**, 1761–1768.
53 J. C. Joyner and J. A. Cowan, *Braz. J. Med. Biol. Res.*, 2013, **46**, 465–485.
54 A. Nicolò, Z. Fantoni and Z. Molphy, *Chem. – Eur. J.*, 2021, **27**, 971–983.
55 S. Leichnitz, J. Heinrich and N. Kulak, *Chem. Commun.*, 2018, **54**, 13411.
56 L. A. Rowe, N. Degtyareva and P. W. Doetsch, *Free Radical Biol. Med.*, 2008, **45**, 1167–1177.
57 A. C. Alves, D. Ribeiro, C. Nunes and S. Reis, *Biochim. Biophys. Acta, Biomembr.*, 2016, **1858**, 2231–2244.
58 L. G. F. Lopes, F. S. Gouveia, A. K. M. Holanda, I. M. M. Carvalho, E. Longhinotti, T. F. Paulo, D. S. Abreu, P. V. Bernhardt, M. A. Gilles-Gonzalez, I. C. N. Diógenes and E. H. S. Sousa, *Coord. Chem. Rev.*, 2021, **445**, 214096.
59 A. Khalid, S. Persano and H. Shen, *Expert Opin. Drug Delivery*, 2017, **14**, 865–877.